Modeling the Tortuosity of Retinal Vessels: Does Caliber Play a Role?

Emanuele Trucco*, Hind Azegrouz, *Member, IEEE*, and Baljean Dhillon

***Abstract*—The tortuosity of retinal blood vessels is a diagnostic parameter assessed by ophthalmologists on the basis of examples and experience; no quantitative model is specified in clinical practice. All quantitative measures proposed to date for automatic image analysis purposes are functions of the curvature of the vessel skeleton. We suggest in this paper that curvature may not be the only quantity involved in modeling tortuosity, and that vessel thickness, or caliber, may also play a role. To support this statement, we devise a novel measure of tortuosity, depending on both curvature and thickness, and test it with 200 vessels selected by our clinical author from the public digital retinal images for vessel extraction database. Results are in good accordance with clinical judgment. Comparative experiments show performance similar to or better than that of four measures reported in the literature. We conclude that there is reasonable evidence supporting the investigation of tortuosity models incorporating more measurements than just skeleton curvature, and specifically vessel caliber.**

***Index Terms*—Automated, curvature, retinal, screening, tortuosity, vasculature properties.**

I. Introduction

A. Tortuosity and Its Clinical Relevance

HEALTHY retinal vessels run in smooth arcs, forming a tree-like network rooted in the optic dics; winding, twisted vessel, are instead a feature of many diseases, including retinopathy of prematurity (ROP), diabetic retinopathy, hypertension, conditions associated with hypoxia [1], and several genetic syndromes. *Tortuosity* is a qualitative parameter used by clinicians to indicate how winding blood vessels are typically on a three- to five-point scale [2].

Measuring tortuosity is important for several reasons. In addition to its association with serious ocular diseases, the close analogy between retinal and cerebral circulations suggests that a deeper understanding of the causes of retinal vascular changes is likely to provide insights into neurovascular pathologies as well [3]. It has been noted that using a grading scale to describe the retinal vasculature significantly improves inter- and intraobserver repeatability [4]. Furthermore, tortuous vessels can potentially inform us about the stresses imposed on the retinal vasculature, and its ability to respond to such stresses. In circulations outside the eye, vessel widening and elongation (leading to tortuosity) are known to be caused by high flow rates [5] and vascular congestion [6]; significant efforts have been put into defining the biophysical parameters needed to cause changes in vascular structure because of their relevance to conditions such as stroke [7]. The etiology of retinal vascular tortuosity can be captured by broad categories, including venous congestion, retinal ischemia, increased blood flow, and rare angiogenesis [8]. In contrast, much detail about the interaction between hemodynamic forces and layers of the vessel wall remains elusive. Mathematical models of angiogenesis have been reported by McDougall *et al.* [9] for tumors, but not, to our knowledge, for retinal vessels. Identification of the mutations responsible for conditions such as familial retinal arteriolar tortuosity [8] could give important information about retinal vessel structure needed for normal circulation. Similarly, knowledge about the amount of sheer stress generated by a given flow rate and vessel curvature would allow one to link degrees of tortuosity with degrees of force acting on the epithelium, which in turn can be associated with cellular responses involving gene transcription and release of mediators [10].

The study and measurement of tortuosity are relevant for both diagnostic and modeling purposes. The key motivation for our study is that tortuosity is a *subjective* clinical judgment; it is therefore plausible that an accurate computational model may need to account for a variety of factors. We propose that computational models of vessel tortuosity ought to incorporate more measurements than just skeleton curvature, and specifically vessel caliber.

B. Quantifying Tortuosity: Related Work

To establish a reliable link between vascular tortuosity and pathologies, it is desirable to define a quantitative, repeatable measure, especially within large, computer-assisted screening programs [11], [12]. A number of quantitative measures have been proposed in the retinal image analysis literature, but it is difficult to establish which one is the most appropriate. There are various reasons for this. First, and most important, tortuosity is not defined quantitatively in the medical literature. Second, the role of tortuosity within diagnosis is hardly quantitative, tortuosity being one of several pieces of information concurring to form a decision. This motivates investigations of different models of the clinical perception of tortuosity. Third, most studies

Manuscript received June 3, 2009; revised October 27, 2009 and February 14, 2010; accepted April 12, 2010. Date of publication May 27, 2010; date of current version August 18, 2010. The work of H. Azegrouz was supported by the British Arab Chamber of Commerce. *Asterisk indicates corresponding author.*

*E. Trucco is with the School of Computing, University of Dundee, Dundee, DD1 4HN, U.K. (e-mail: manueltrucco@computing.dundee.ac.uk).

H. Azegrouz is with the Spanish National Centre of Cardiovascular Research, 28029 Madrid, Spain (e-mail: hazegrouz@cnic.es).

B. Dhillon is with the NHS Princess Alexandra Eye Pavilion, Edinburgh EH3 9HA, U.K., and also with the University of Edinburgh, Edinburgh EH8 9YL, U.K. (e-mail: bal.dhillon@luht.scot.nhs.uk).

Color versions of one or more of the figures in this paper are available online at http://ieeexplore.ieee.org.

Digital Object Identifier 10.1109/TBME.2010.2050771

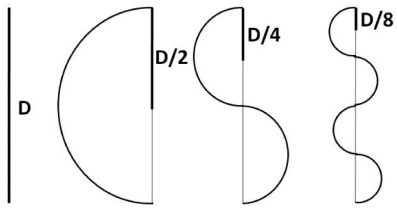

Fig. 1. Circular arc has the same DM value as a curve formed by an arbitrary number N of circular arcs spanning the same chord: $\pi D/2 = \cdots = N(\pi D/2N)$. The latter, however, are perceived as increasingly more tortuous than the former.

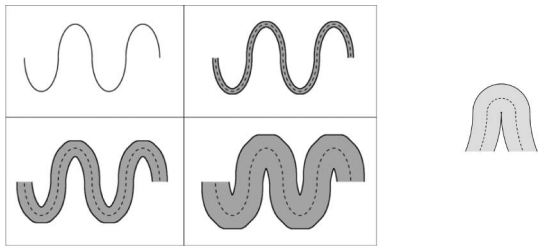

Fig. 2. Left: Four curves with the same skeleton but different thickness. Right: Thickness limits skeleton bending, i.e., the maximum curvature achievable.

compare automatic results with the answers of a single clinician (this paper is no different in that regard), but clinical judgment varies with clinicians. Finally, no database of test images with widely accepted ground-truth exists yet for tortuosity, so that it is impossible to compare results on a wide, common basis. Notice that such databases exist in other parts of the image analysis community, for instance, face analysis [13] and stereo [14]. A classification of reported methods is given shortly. One method, which does not fall in our classification, is due to Patasius *et al.* [15], who presented a finite-element model of vessel deformation under varying blood pressure and studied the behavior of several tortuosity measures with synthetic vessels.

The *distance metric* (DM) is defined as the ratio between the length of the vessel and that of the chord joining the vessel's end points. It has been widely used as a tortuosity measure; for instance, Heneghan *et al.* [16] used it with width information to decide if a subject with ROP needed treatment. Swanson *et al.* [17] compared retinal blood vessels close to the optic disc in full-term and preterm infants, with and without ROP. They recorded venular diameter, arteriolar diameter, and tortuosity. They detected significant increases in arteriolar tortuosity with increasing ROP severity. Wood *et al.* [18] evaluated the differences in properties of superficial femoral artery (SFA) for men and women in term of curvature and tortuosity, using the DM. SFA in men were significantly more curved and tortuous than in women.

The main problem of the DM as a tortuosity measure is that it assigns the same value to an intuitively very tortuous curve as to a simple, gentle arc with the same average deviation from the chord (see Fig. 1). This is because the DM is simply a measure of deviation from a straight line (a global measure), whereas tortuosity seems more directly related to local measures like curvature. For this reason, Smedby *et al.* [19] introduced a measure multiplying the DM by the number of the inflection points found within a vessel. Bullit *et al.* [20] applied a similar measure to 3-D data. They searched for curvature maxima of 3-D vessels, approximating curvature with the discrete variation of the normal direction to the vessel between subsequent vessel voxels. Their method recognized two of the three types of abnormal tortuosity of intracerebral vessels; their three types of abnormal tortuosity were based on length, amplitude, and frequency at which vessels twist.

Discrete-derivative measures are based on the differences between the gradients at successive vessel points (samples). Dougherty and Varro [21] define a tortuosity coefficient as the sum of the differences between the gradients of two successive points divided by the sampling interval. Eze *et al.* [22] introduced a similar measure that they tested using synthetic, 2-D sine wave simulations, showing better performance than the DM. Chandrinos *et al.* [23] computed the average of the angles between segments joining subsequent pairs of sample points in the vessel skeleton.

Curvature-based measures are integral functions of curvature estimates along the vessel's skeleton, often weighted sums of absolute or squared curvatures. Hart *et al.* [2] compared seven such measures using two classification problems, classifying blood vessel segments as tortuous or nontortuous, and classifying the whole vessel network. They found the total squared curvature measure to yield the closest results to the ophthalmologist's notion of tortuosity. The measure was defined as the integral of the squared curvature along the vessel's skeleton. Grisan *et al.* [24] partitioned each vessel into segments of constant-sign curvature and combined the number of such segments and their curvature values. A normalization factor was introduced allowing comparison of vessels of different lengths. Their results with a set of 60 vessels showed higher correlation with medical judgment compared with methods proposed by Hart *et al.* [2]. Bullit *et al.* [20] introduced a measure based on 3-D curvature, estimated via a geometric method. Their measure performed particularly well in detecting tight coils.

C. Tortuosity and Vessel Thickness

All measures proposed, to our best knowledge, represent blood vessels as 1-D curves and posit a direct dependency on skeleton curvature alone. Our main tenet is that the perceived tortuosity of blood vessels may depend on other factors as well, of which we investigate thickness. To illustrate intuitively the potential role of thickness, Fig. 2 (left) shows four vessels with the same skeleton but different thickness. Our hypothesis is based on the observation that thicker vessels have thicker walls than thinner ones; hence achieving a given skeletal curvature requires more effort for thicker vessels than for thinner ones. Notice that vessel thickness affects also the maximum allowable curvature of the skeleton, which depends inversely on thickness Fig. 2 (right). Recent biomechanical models seem to encourage our intuition. Han [25] presented a biomechanical model of arterial buckling. Using an elastic cylindrical arterial model, the critical buckling pressure was found to be indeed a function of wall

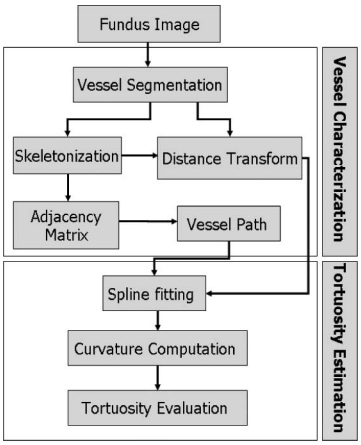

Fig. 3. Architecture of our tortuosity estimation system.

thickness, together with wall stiffness, arterial radius, length, and axial strain.

Our proposed measure combines curvature and thickness, extending reported measures [2], [16], [24] based solely on skeleton curvatures. It is defined as a weighed Minkowski norm of the curvatures along the vessel boundaries, and is an increasing function of vessel diameter (thickness).

D. System Outline

We have implemented a tortuosity estimation system organized in two stages: 1) vessel location and characterization (Section II) and 2) estimation of vessel tortuosity, using our thickness-dependent measure (Section III). Fig. 3 captures the system architecture at a glance.

II. Location and Characterization of Target Vessels

The purpose of the first stage is to provide the user with an efficient tool for selecting vessel segments for tortuosity analysis. The input is a retinal image; the output is a representation of the vessel selected by the user, including skeleton and local radii. Our discussion follows the architecture, as shown in Fig. 3.

A. Segmentation

Any tortuosity measure requires a preliminary step locating the retinal vasculature, i.e., generating a vasculature map. Fig. 4(a) shows an example of the images we used; further details are given in Section V-A.

A region of interest (ROI) containing the vessels for which tortuosity is to be estimated is selected manually using a GUI. The same tool allows vessel selection and is used by the clinician to create a set of vessel to be analyzed. All subsequent operations take place within the ROI. This has the only purpose of speeding up computation and does not affect tortuosity estimation.

B. Skeletonization

The skeleton of the vascular network is obtained from the segmented binary image by a thinning process. Pixels are eliminated from the boundaries toward the center preserving the eight-neighbor connectivity [26]. Local radii are then estimated at each skeleton point by computing the point's Euclidean distance from the nearest background pixel, using the distance transform. Radii values are then associated to skeleton pixels for later use. The skeletonization result for the input image in Fig. 4(a) is shown in Fig. 4(b) (left and right).

C. Branching and Terminal Nodes Detection

Terminal and branching points are detected using the skeleton image. We count the number t of transitions from black to white moving clockwise around the eight neighborhood of a point, and use this number to classify the point as terminal node ($t = 1$), nonsignificant point ($t = 0, 2$), or branching point ($t \geq 3$). Results for the example mentioned earlier are shown in Fig. 4(b) (left).

D. Representing the Vessel Graph: Adjacency Matrix

We now have the skeleton structure of the vasculature inside the ROI. To compute the adjacency matrix representing the graph of the vasculature skeleton, we consider all branching and terminal points as vertexes, and find which vertexes are connected by arcs. We delete the graph vertexes (Fig. 4(b), left) from the skeleton image, and all pixels in their eight neighborhood. The connected components (regions) in the resulting image L are the arcs (edges) of the graph and are given numerical labels. Two vertexes are connected if they lie at the end points of a constant-label component (i.e., arc) of L. We then number all the vertexes of the graph and build an adjacency matrix M_C, in which $M_C(i,j) = 1$ if vertexes i and j are connected, i.e., belong to the same arc, and $i \neq j$. Moreover, $M_C(i,j) = \infty$ if i and j are not connected; $M_C(i,j) = 0$ if $i = j$; $M_C(i,j) = M_C(j,i)$, as connectivity is symmetric.

III. Estimation of Vessel Tortuosity

The purpose of the second stage is to generate tortuosity estimates for the vessels selected by the user. The input is the representation of the target vessel (skeleton and local radii) generated by the first stage. The output is a real-number quantifying tortuosity. The range of this number depends inversely on an integer parameter, $p \in [1, 4]$, defined in the next section; in our experiments, the range varied from about 0.1 for $p = 1$ to 0.0025 for $p = 4$. This range must be partitioned to model a given number of tortuosity classes, as done in clinical practice.

A. Boundary Localization and Curvature Estimation

Many shape representations have been proposed for 2-D contours; we refer the reader to Zhang and Lu's review [27]. Here, we use simply an ordered sequence of points to represent the axis of a vessel, and a local spline approximation to counteract the effect of quantization and other noise sources when estimating curvatures [28].

The two boundary pixels associated to each skeleton (axis) point are computed as follows (see Fig. 5). Consider a vessel skeleton $S = \{\mathbf{s}(1), \ldots, \mathbf{s}(N)\}$, with $\mathbf{s}(k) = (x_s(k), y_s(k))$. The normal to the axis at $\mathbf{s}(k)$ intersects the two boundary

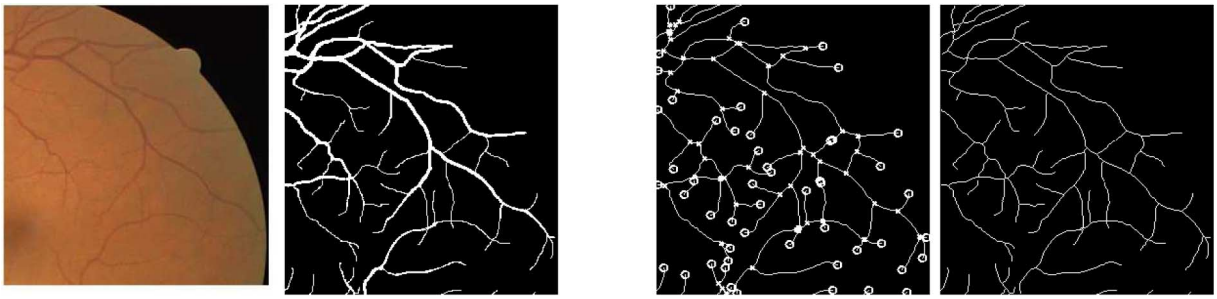

(a) (b)

Fig. 4. (a) Left: fundus image (DRIVE set), (a) right: binary vasculature map. (b) Left: skeleton with branching and end points highlighted. (b) Right: extracted skeleton.

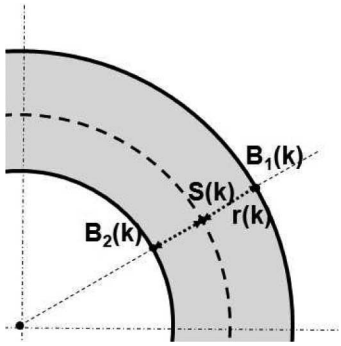

Fig. 5. Skeleton point and associated boundaries points.

contours in two points, $\mathbf{B}_1(k)$ and $\mathbf{B}_2(k)$ (see Fig. 5), where $\mathbf{B}_j(k) = (x_j(k), y_j(k))$ and $j = 1, 2$. Let $r(k)$ be the radius (half-width) of the cross section thus defined; the coordinates of the boundary points are (omitting k for simplicity)

$$x_j = x_s \mp \frac{r y_s'}{\sqrt{x_s'^2 + y_s'^2}} \qquad y_j = y_s \pm \frac{r x_s'}{\sqrt{x_s'^2 + y_s'^2}} \tag{1}$$

where $j = 1, 2$ and prime indicates differentiation with respect to the curve parameter.

It is well-known that curvature estimation from discrete samples is an ill-posed problem that can be approached by the introduction of a regularization procedure. Smoothing the contour coordinates, e.g., using a Gaussian kernel, is a simple but often effective solution. A second approach is local interpolation, typically fitting locally smooth curves.

Here, we estimate curvature by interpolation with cubic B-splines. We refer the reader to [29] for the formulae involved and to [28] for a discussion on the numerical estimation of curvature. A support window of 5 pixels achieved an adequate compromise between locality and noise attenuation in our experiments with DRIVE images. The window size was determined experimentally, by observing the curvature values obtained with vessel contours over windows of size 3, 5, 7, and 9. This figure would of course need revising for different image resolutions. In essence, smaller windows lead to excessively noisy measurements; larger windows tend to underestimate curvature values.

B. Thickness-Dependent Tortuosity Measure

To compare results with previously reported work, we begin by defining a measure depending on skeleton curvature only. This measure generalizes the square-root mean value of axis curvatures identified as the best performer in the study by Hart *et al.* [2], and is defined by

$$\tau_s(\kappa_s, p) = \left(\sum_j |\kappa_s(j)|^p \right)^{\frac{1}{p}} \tag{2}$$

where p is a strictly positive integer, and $\kappa_s(j)$ is the curvature at the jth point of the vessel skeleton. Choosing a value for p is discussed in Section IV. Notice that, for $p = 2$, τ_s becomes the measure recommended by Hart *et al.*

As stated in Section I, we postulate that perceived tortuosity might increase with thickness. We notice that the curvatures of the boundary points $\mathbf{B}_1(k)$ and $\mathbf{B}_2(k)$ associated to a skeleton point $\mathbf{s}(k)$ are different, apart from the case of locally linear boundaries. We use this fact to define a measure combining curvature and thickness defined as the p-mean root of the averaged p-powers of the curvatures of pairs of corresponding boundary points:

$$\tau_t(\kappa_{B1}, \kappa_{B2}, p) = \left(\sum_j \frac{|\kappa_{B1}(j)|^p + |\kappa_{B2}(j)|^p}{2} \right)^{\frac{1}{p}} \tag{3}$$

where κ_{B1} and κ_{B2} are, respectively, the boundary curvatures at the two boundary points associated with the jth skeleton point. We now illustrate three properties of this definition. For simplicity, we drop from the notation the explicit dependency of τ_t, τ_s on κ and p.

Property 1: If the vessel width is zero, $\tau_t = \tau_s$.

Proof: Trivial from definitions, (2) and (3), as in this case the vessel coincides with its skeleton. This implies that τ_s can be regarded as a special case of τ_t.

Property 2: The function τ_t *increases with the local radius*, $r(k)$.

Proof: Without loss of generality, we assume a locally constant radius, $r(k) = D$. We first prove that τ_t increases with D when the skeleton is an arc of a circle of radius R_0 ($D \leq R_0$), then we generalize to any C^2 curve. Summations over j are

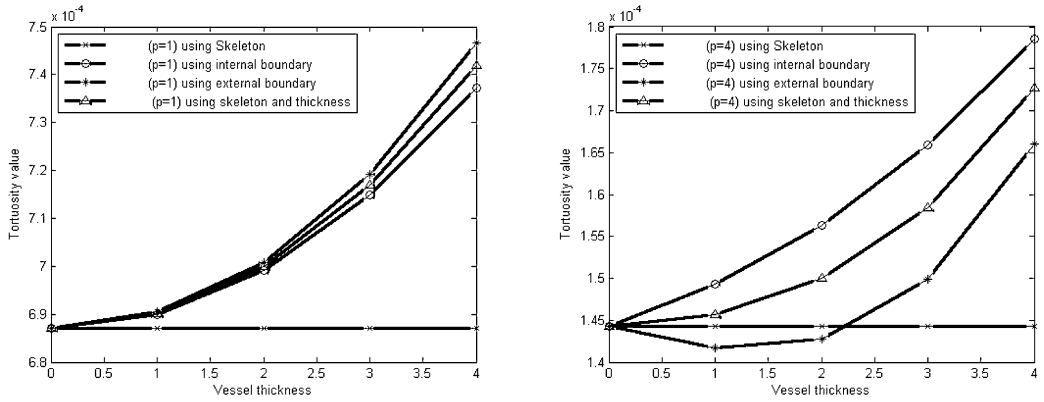

Fig. 6. Illustration of Property 2 (see text), showing tortuosity increasing with thickness for synthetic vessel with fixed skeleton. Tortuosity values are plotted against vessel radius for $p = 1$ (left) and 4 (right). The plots show τ_s values for the vessel axis (crosses), for the two vessel boundaries (circles, stars), and τ_t (triangles) for the vessel segment.

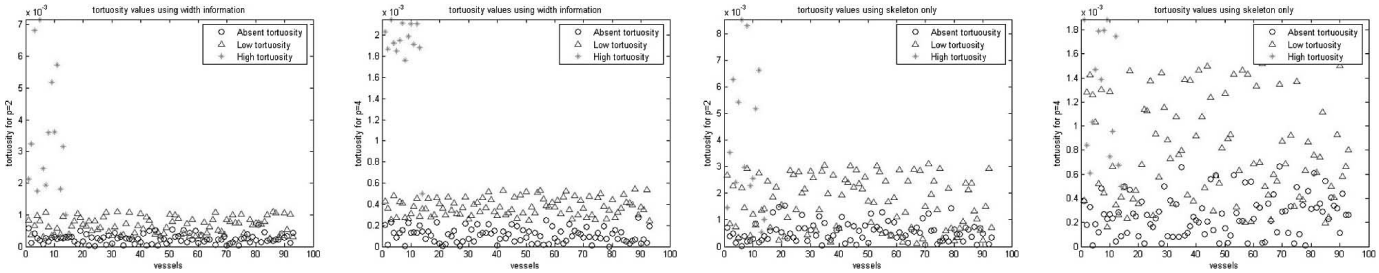

Fig. 7. Class separation achieved by our tortuosity measure (left) is better than the one achieved by the skeleton-based measure (right) with 200-vessel sample. The effect increases with p (shown here: $p = 2$ and $p = 4$).

intended over all skeleton points. Let δ be the length of a small skeleton arc, and refer to $\mathbf{B}_1, \mathbf{B}_2$, the inner and outer boundary points associated with the kth skeleton point. As the skeleton is locally circular, we have (see Fig. 5)

$$\kappa_{B1} = \frac{1}{R_0 - D} \quad \kappa_{B2} = \frac{1}{R_0 + D} \quad \kappa_s = \frac{1}{R_0}. \tag{4}$$

Therefore, as $D < R_0$,

$$\begin{aligned}\tau_t &= \left(\frac{1}{2}\right)^{1/p} \left(\sum_j \left|\frac{1}{R_0 - D}\right|^p + \left|\frac{1}{R_0 + D}\right|^p\right)^{\frac{1}{p}} \\ &= \left(\frac{1}{2}\right)^{1/p} \left(\sum_j \left(\frac{1}{R_0 - D}\right)^p + \left(\frac{1}{R_0 + D}\right)^p\right)^{\frac{1}{p}} \\ &= \left(\frac{\delta}{2}\right)^{1/p} \frac{R_0}{R_0^2 - D^2} \left(\sum_{2k=0}^{2k<=p} C_p^{2k} \left(\frac{D}{R_0}\right)^{2k}\right)^{\frac{1}{p}} \end{aligned} \tag{5}$$

where C_p^{2k} is the binomial coefficient of p and $2k$ (the number of combinations of $2k$ elements chosen among p ones).

The last expression obtained for τ_t is an increasing function of D (see shortly). This result generalizes to any C^2 curve, considering that, locally, the curve is coincident with an arc of its osculating circle.

Property 3: For high values of the boundary curvatures, τ_t is an increasing function of p and vice versa.

Proof: This follows from the definition of τ_t, (3): as p is a strictly positive integer, the larger the value of $|\kappa_{B1}(j)|$ and $|\kappa_{B2}(j)|$, the larger the contribution of the polynomially increasing term to the tortuosity value.

We illustrate Property 2 in Fig. 6, using synthetic vessels built around the skeleton of a real vessel. Each graph plots four curves against thickness: τ_t, τ_s for the vessel axis, and τ_s for the two boundary contours. For reasons of space, we show graphs only for $p = 1$ and $p = 4$ ($p = 2$ yields one of the measures used by Hart *et al.* [2]). We see that τ_t (indeed all measures) increases with thickness (Property 2), as desired, the tortuosity of the skeleton is constant, as independent of thickness. Notice also that the combined measure τ_t always falls between the curvature-only tortuosity of the two vessel boundaries.

In the conditions of Property 3, as τ_t becomes an increasing function of p, the difference between the tortuosity estimates of two vessels computed with p_1 and $p_2 > p_1$ will be larger when p_2 is used. This fact can be used to identify a best value for p for tortuosity classification. We discuss this further in Section IV, in the context of choosing a value for p to classify tortuosity in a given number of classes. We notice also that Fig. 7 shows that our tortuosity measure increases with increasing vessel thickness.

C. Classification Scheme

To assign vessels to one of three tortuosity classes, it is necessary to divide the range of the measures into three regions, i.e., to adopt a classification scheme. To facilitate comparison with previous work, we adopted the *logistic regression model* used by Hart *et al.* [2] in their influential study. We give a short account of the logistic model here and refer the reader to [30] for details.

The logistic regression model is a discriminative classification scheme. Given a set of K classes $C_1, \ldots, C_K$ and a data vector $\mathbf{x}$ of feature values or function thereof, the model assumes class-conditional distributions $f(\mathbf{x}|C_k)$ belonging to the exponential family, so that the posterior class distributions $f(C_k|\mathbf{x})$ can be written as generalized linear functions of linear combinations of the feature values. For a 2-class problem, this function is a logistic sigmoid; for more classes, as in our case, the *softmax function*

$$f(C_k|\mathbf{x}) = \frac{e^{\mathbf{w}_k^\top \mathbf{x}}}{\sum_{j=1}^{K} e^{\mathbf{w}_j^\top \mathbf{x}}}$$

where $\mathbf{w}_j, \mathbf{w}_k$ are vectors of weights. In our case, we have only one feature, the tortuosity value x, and three classes ($K = 3$), so that the previous equation specializes to

$$f(C_k|x) = \frac{e^{w_0 + w_1 x}}{\sum_{j=1}^{3} e^{w_{j0} + w_{j1} x}}.$$

The weights are determined by maximum likelihood. The likelihood function is

$$f(\mathbf{T}|\mathbf{w}) = \prod_{n=1}^{N} \prod_{k=1}^{3} p(C_k|x)^{t_{nk}},$$

where N is the number of examples used, k spans the three classes, and t_{nk} are target variables, taking values 1 if x belongs to class C_k and 0 otherwise. It has been proven that this ML problem is concave, and its unique solution is determined efficiently by iterative reweighted least squares, a Newton-Raphson iterative algorithm [30].

D. Selecting a Value for p

Increasing p has the effect of creating clearer clusters as the tortuosity difference between two given vessels increases (Section III): Fig. 7 (left) illustrates this idea with the 200-vessel sample used in our experiments: class separation is better for $p = 4$ than $p = 2$ (plots for other values omitted for reasons of space). For comparison, Fig. 7(right) shows that clusters are not separated as clearly with the skeleton-based measure (2). However, p cannot be simply increased indefinitely to improve classification. To see this, we built confusion matrices for results achieved in a p range from 1 to 10, and plotted classification rates as functions of p for vessels in each of the three classes (see Fig. 8). Table I reports the classification rates, i.e., the proportion of the total number of predictions that were correct in the given p range (the observed rates for $p = 8, 9, 10$, not shown, were the same as for $p = 7$). The highest classification accuracy over increasing values of p is achieved for $p = 4$. Fig. 8 shows that the best classification rate for the three classes simultaneously is achieved for $p = 4$. Increasing further the value of p decreases the classification rate of at least one class. These observations form the basis on which $p = 4$ is declared the best value. This is probably due to the fact that the maximum value of the target measure for our dataset decreases with p (for $p = 3$, it is 0.004, for $p = 4$, it is 0.0025), so that for $p > 4$ the numerical noise confounds the classifier. This result applies, strictly speaking, to the set of 200 vessels analyzed, which was however chosen to include an ample spectrum of real tortuosity cases. For completeness, we observe that (3) and (4) suggest that for p tending to infinity the measure tends to the sum of the maximum tortuosity of each point. In practice, it seems sensible to use small values for p, leading to good classification values (see above).

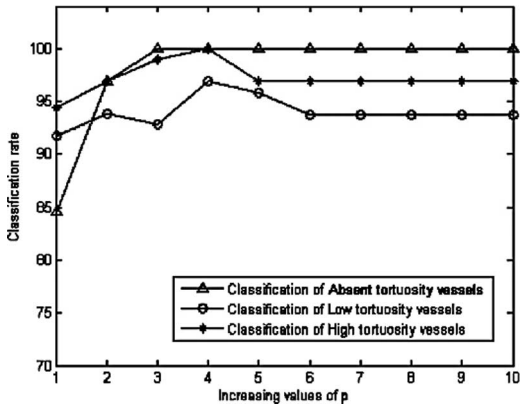

Fig. 8. Classification of tortuosity for increasing values of p with the 200 vessels used in our tests.

TABLE I
CLASSIFICATION ACCURACY OF OUR TORTUOSITY MEASURE FOR DIFFERENT VALUES OF p

p	1	2	3	4	5	6	7
Accuracy	93.33	95.56	96.63	98.21	97.42	95.72	95.72

Ground truth labels are columns, algorithms labels rows.

IV. RESULTS

A. Experimental Setup and Procedure

We carried out *K*-fold cross-validation tests with a set of 200 vessels selected manually from 20 images, 10 vessels per image, from the public DRIVE set [31]. The vessels were chosen by the clinical author (Dhillon), an experienced practicing ophthalmologist, balancing the number of vessels in each class. We used larger caliber and mainly first-order arterioles and venules to obtain a complete spectrum of tortuosity. Our choice was based on the assumption that the larger vessels inform the subjective assessment by the clinician on a first-pass scan. The images were acquired with a Canon CR5 nonmydriatic 3-CCD camera with 45° field of view. Each image was 768×584 pixels. Fig. 9 shows an example. Thickness (vessel diameter) estimates were obtained as the widths of the vessels in the DRIVE vessel masks, which were validated by Staal *et al.* [31].

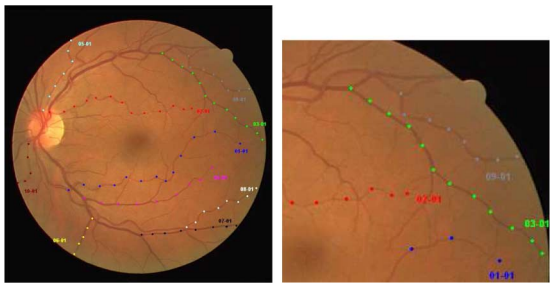

Fig. 9. Example of a DRIVE image with identified vessels of different tortuosity and magnification of a region (the captions are immaterial for the discussion).

The vessel set was randomly divided into 20 subgroups containing 10 vessels each. In each of 20 runs, training was performed to determine the weights (Section IV-C) on 190 vessels and tested on 10, leaving out a different 10-vessel group each time. The figures reported below are averaged over the 20 runs. Thickness (vessel diameter) estimates were obtained as the widths of the vessels in the DRIVE vessel masks, which were validated by Staal *et al.* [31].

Vessels were identified on the image, using a GUI by clicking two points on the vasculature tree. If there was no branching node between the points, the target segment was simply the graph arc containing the two points; otherwise, the segment was given by the shortest path between the two points, estimated by Dijkstra's algorithm, using the adjacency matrix (Section II-D).

Following normal practice in the literature, we assessed the performance of our thickness-dependent measure against clinical judgment. The tortuosity of each vessel was assessed by our clinical author as belonging to one of three levels (absent, low, high tortuosity). The three-level scale is a common choice in clinical practice, although a few authors report using a 5-level scale, e.g., [4].

We compared results with five measures reported in the literature: the DM, two of Harts curvature-only measures (the best-performing one described earlier, called τ_3 in [2], and the second best, called τ_2, the sum of the absolute values of the curvature along the vessel), and the measures suggested by Grisan *et al.* [24] and Chandrinos *et al.* [23]. Confusion matrices were used throughout and all experiments conducted with our own implementations of the various measures. In our confusion matrices, each row gives the percentages of the vessels classified by the system in this row (e.g., high) that were classified in each class (absent, low, high) by the clinician. Therefore, the entries of each row sum up to 100, but the columns do not need to.

Comparisons are not straightforward as different measures have different parameters. For instance, Chandrinos *et al.* measure [23] include a parameter, the quantization step along the vessel, the value of which is not discussed. The authors state however that a vessel of 10 pixels or less is considered too short for computing tortuosity; we therefore used a step of 5 in our tests and only vessels longer than 10 pixels. We implemented Grisan's method with and without an hysteresis threshold [24]. The best results were achieved with hysteresis, using a threshold value of 2×10^{-4}. Hart's measures, τ_2 and τ_3, depend only on the curvatures of the vessels axis and contain no parameters.

TABLE II
CLASSIFICATION PERFORMANCE AS CONFUSION MATRICES

$\tau_t, p = 1$	**Clinical** Absent	**Ground** Low	**Truth** High
Absent	$96.4 \pm 1.03\%$	$3 \pm 3.06\%$	$0.6 \pm 2.16\%$
Low	$7.2 \pm 1.32\%$	$91.6 \pm 2.15\%$	$1.2 \pm 0.93\%$
High	0%	14.2%	85.8%
$\tau_t, p = 2$			
Absent	$96.9 \pm 1.94\%$	$2.0 \pm 1.02\%$	$1.1 \pm 1.83\%$
Low	$2.9 \pm 0.22\%$	$94.1 \pm 0.77\%$	$3.0 \pm 2.21\%$
High	0%	2.8%	97.2%
$\tau_t, p = 3$			
Absent	$99.2 \pm 1.0\%$	$0.8 \pm 1.21\%$	$0 \pm 0.11\%$
Low	$2.9 \pm 0.37\%$	$93.8 \pm 2.2\%$	$2.03 \pm 0.71\%$
High	$0.0 \pm 0.0\%$	$0.0 \pm 0.0\%$	$100 \pm 0.0\%$
$\tau_t, p = 4$			
Absent	$100 \pm 0.0\%$	$0.0 \pm 0.0\%$	$0.0 \pm 0.0\%$
Low	$1.6 \pm 0.2\%$	$97.3 \pm 1.88\%$	$1.1 \pm 1.02\%$
High	$0.0 \pm 0.0\%$	$6.8 \pm 1.4\%$	$93.2 \pm 0.33\%$
Hart τ_3			
Absent	$88.2 \pm 2.77\%$	$10.0 \pm 3.09\%$	$1.8 \pm 2.68\%$
Low	$7.2 \pm 2.17\%$	$86.9 \pm 2.09\%$	$5.9 \pm 3.12\%$
High	$6.7 \pm 2.0\%$	$32.1 \pm 3.24\%$	$61.2 \pm 3.11\%$
Hart τ_2			
Absent	$81.7 \pm 3.88\%$	$13.8 \pm 3.0\%$	$4.5 \pm 3.75\%$
Low	$8.1 \pm 2.09\%$	$81.3 \pm 3.0\%$	$10.6 \pm 2.97\%$
High	$10.6 \pm 3.77\%$	$26.5 \pm 3.11\%$	$62.9 \pm 4.0\%$
Dist metr			
Absent	$90.8 \pm 3.49\%$	$9.2 \pm 2.93\%$	$0.0 \pm 0.0\%$
Low	$16.3 \pm 2.56\%$	$69.2 \pm 3.0\%$	$14.5 \pm 2.88\%$
High	$12.4 \pm 2.67\%$	$25.3 \pm 3.99\%$	$62.3 \pm 3.61\%$
Chandr			
Absent	$82.3 \pm 2.1\%$	$12.4 \pm 1.99\%$	$5.3 \pm 1.75\%$
Low	$6.2 \pm 2.33\%$	$83.7 \pm 1.64\%$	$10.1 \pm 2.0\%$
High	$1.0 \pm 2.38\%$	$5.9 \pm 2.41\%$	$93.1 \pm 2.0\%$
Grisan			
Absent	$80.5 \pm 2.55\%$	$6.2 \pm 1.89\%$	$13.3 \pm 3.11\%$
Low	$9.8 \pm 2.0\%$	$76.7 \pm 3.01\%$	$13.5 \pm 2.51\%$
High	$0 \pm 0.0\%$	$3.0 \pm 1.99\%$	$97.0 \pm 2.53\%$

B. Classification Results

Table II shows the confusion matrices comparing automatic classifications with clinical judgment. We show results for our thickness-dependent measure with p values from 1 to 4, for the measures proposed by Hart (τ_2 and τ_3), Grisan, and Chandrinos, and for the DM. Measures depending on curvature only are of course applied to the vessel skeleton.

V. CONCLUSION AND FUTURE WORK

We propose that the clinical perception of tortuosity may depend on factors beyond geometric properties of the vessels axis. On this basis, we have tested a quantitative measure combining vessel caliber and curvature against clinical judgment with 200 vessels selected and graded by an experienced clinician. Our measure proved in very good agreement with medical judgment, indeed generally better than that of five other measures proposed in the literature. This assessment remains within the boundaries of our experimental setup: annotations from a single clinician, a set of 200 vessels (large in comparison with several computational studies reported, but still limited for general conclusions), and own, independent implementation of other

authors' methods (the results of which we regard therefore as strongly indicative only). Understanding the ultimate value of our measure for diagnosis and clinical practice goes well beyond the scope of this paper and will require further study in clinical disease assessment and prognostication.

We do not claim that our measure outperforms others necessarily, but that tortuosity models may need to include factors other than axis curvature alone. It seems indeed plausible that an accurate computational model may need to account for a variety of factors, perhaps even nongeometric ones like training, previous experience, and purpose of the diagnosis (e.g., interventional or not). This is part of our future research plans, which also include further validation using larger vessel samples, judgment from multiple clinicians, and a firmer understanding of the diagnostic value of automatic tortuosity measures.

ACKNOWLEDGMENT

The authors would like to thank Optos plc, C. Buchanan, D. Cairns, P. Wilson, J. Ellis, and T. McGillivray for support and helpful discussions.

REFERENCES

[1] J. McCrary, "Venous stasis retinopathy of stenotic or occlusive carotid origin," *J. Clin. Neuro-Ophthalmol.*, vol. 9, no. 3, pp. 195–199, 1989.

[2] W. Hart, M. Goldbaum, B. Cote, P. Kube, and M. Nelson, "Measurement and classification of retinal vascular tortuosity," *Int. J. Med. Inf.*, vol. 53, pp. 239–252, Feb. 1999.

[3] N. Patton, T. Aslam, T. MacGillivray, A. Pattie, I. Deary, and B. Dhillon, "Retinal vascular image analysis as a potential screening tool for cerebrovascular disease: A rational based on homology between cerebral and retinal microvasculatures," *J. Anat.*, vol. 206, pp. 319–348, 2005.

[4] J. Wolffsohn, G. Napper, S. Ho, A. Jaworski, and T. Pollard, "Improving the description of the retinal vasculature and patient history taking for monitoring systemic hypertension," *Ophthalmic Physiol. Opt.*, vol. 21, no. 6, pp. 441–449, 2001.

[5] E. Sho, H. Nanjo, M. Sho, M. Kobayashi, M. Komatsu, K. Kawamura, C. Xu, C. Zarins, and H. Masuda, "Arterial enlargement, tortuosity, and intimal thickening in response to sequential exposure to high and low wall shear stress," *J. Vasc. Surg.*, vol. 39, no. 3, pp. 601–612, 2004.

[6] M. Bernard, I. Chazana, M. Balodimosa, D. Holsclawa, and H. Shwachman, "Microcirculation in young adults with cystic fibrosis: Retinal and conjunctival vascular changes in relation to diabetes," *J. Pediatr.*, vol. 77, no. 1, pp. 86–92, 1970.

[7] G. Hademenos and T. Massoud, "Biophysical mechanisms of stroke," *Stroke (Amer. Heart Assoc.)*, vol. 28, no. 10, pp. 2067–2077, 1997.

[8] F. Sutter and H. Helbig, "Familial retinal arteriolar tortuosity: A review," *Surv. Ophthalmol.*, vol. 48, no. 3, pp. 245–255, 2003.

[9] S. R. McDougall, A. R. A. Anderson, and M. A. J. Chaplain, "Mathematical modelling of dynamic adaptive tumour-induced angiogenesis: Clinical implications and therapeutic targeting strategies," *J. Theor. Biol.*, vol. 241, pp. 564–589, 2006.

[10] T. Ishida, M. Takahashi, M. Corson, B. Berk, M. J. Gimbrone, R. Alexander, and J. Strong, "Fluid sheer stress-mediated signal transduction: How do endothelial cells transduce mechanical force into biological responses?" *Ann. New York Acad. Sci.*, vol. 811, pp. 12–23, 1997.

[11] M. Brown, S. Shah, R. Pais, L. Yeng-Zhong, M. McNitt-Gray, J. Goldin, A. Cardenas, and D. Aberle, "Database design and implementation for quantitative image analysis research," *IEEE Trans. Inf. Technol. Biomed.*, vol. 9, no. 1, pp. 99–108, Mar. 2005.

[12] P. Krause, J. Fox, M. O'Neil, and A. Glowinski, "Can we formally specify a medical decision support system?" *IEEE Expert*, vol. 8, no. 3, pp. 56–61, Jun. 1993.

[13] The facial recognition technology (feret) database. (2009). [Online]. Available: http://www.itl.nist.gov/iad/humanid

[14] The middlebury stereo vision page. (2009). [Online]. Available: http://vision.middlebury.edu/stereo/

[15] M. Patasius, V. Marozas, Lukosevicius, and D. Jegelevicius, "Model based investigation of retinal vessel tortuosity as a function of blood pressure: preliminary results," in *Proc. 29th IEEE Eng. Med. Biol. Conf. (EMBC 2007)*, pp. 6459–6462.

[16] C. Heneghan, J. Flynn, M. OKeefe, and M. Cahill, "Characterization of changes in blood vessel width and tortuosity in retinopathy of prematurity using image analysis," *Med. Image Anal.*, vol. 6, pp. 407–429, Dec. 2002.

[17] C. Swanson, K. D. Cocker, K. H. Parker, M. J. Moseley, and A. R. Fielder, "Semiautomated computer analysis of vessel growth in preterm infants without and with rop," *Br. J. Ophthalmol.*, vol. 87, pp. 1474–1477, 2003.

[18] N. B. Wood, S. Z. Zhao, A. Zambanini, M. Jackson, W. Gedroyc, S. A. Thom, A. D. Hughes, and X. Y. Xu, "Curvature and tortuosity of the superficial femoral artery: A possible risk factor for peripheral arterial disease," *J. Appl. Physiol.*, vol. 101, pp. 1412–1418, 2006.

[19] O. Smedby, N. Hogman, S. Nilsson, U. Erikson, A. G. Olson, and G. Walldius, "Two dimensional tortuosity of the superficial femoral artery in early atherosclerosis," *J. Vasc. Res.*, vol. 30, pp. 181–191, 1993.

[20] E. Bullitt, G. Gerig, S. Pizer, W. Lin, and S. Aylward, "Measuring tortuosity of the intracerebral vasculature from mra images," *IEEE Trans. Med. Img.*, vol. 22, no. 9, pp. 1163–1171, Sep. 2003.

[21] G. Dougherty and J. Varro, "A quantitative index for the measurement of the tortuosity of blood vessels," *Med. Image Anal.*, vol. 22, no. 8, pp. 567–574, 2000.

[22] C. U. Eze, R. Gupta, and D. L. Newman, "A comparison of quantitative measures of arterial tortuosity using sine wave simulations and 3d wire models," *Phys. Med. Biol.*, vol. 45, pp. 2593–2599, 2000.

[23] K. Chandrinos, M. Pilu, R. Fisher, and P. Trahanias, "Image processing techniques for the quantification of atherosclerotic changes," in *Proc. Mediterr. Conf. Med. Biol. Eng. Comp.*, 1998.

[24] E. Grisan, M. Foracchia, and A. Ruggeri, "A novel method for the automatic evaluation of retinal vessel tortuosity," *IEEE Trans. Med. Img.*, vol. 27, no. 3, pp. 310–319, Mar. 2008.

[25] H.-C. Han, "A biomechanical model of artery buckling," *J. Biomech.*, vol. 40, no. 16, pp. 3672–3678, 2007.

[26] L. Lam, S. W. Lee, and C. Suen, "Thinning methodologies: A comprehensive survey," *IEEE Trans. Pattern Anal. Mach. Intell.*, vol. 14, no. 9, pp. 879–884, Sep. 1992.

[27] D. Zhang and G. Lu, "Review of shape representation and description techniques," *Pattern Recognit.*, vol. 37, pp. 1–19, 2004.

[28] G. Medioni and Y. Yasumoto, "Corner detection and curve representation using cubic b-splines," in *Proc. IEEE Int. Conf. Robot. Autom.*, 1986, vol. 3, pp. 764–769.

[29] L. Piegl and W. Tiller, *The NURBS Book*. New York: Springer-Verlag, 1997.

[30] C. M. Bishop, *Pattern Recognition and Machine Learning*. New York: Springer-Verlag, 2006.

[31] J. J. Staal, M. D. Abramoff, M. Niemeijer, M. A. Viergever, and B. van Ginneken, "Ridge based vessel segmentation in color images of the retina," *IEEE Trans. Med. Imag.*, vol. 23, no. 4, pp. 501–509, Apr. 2004.

Emanuele Trucco received the M.Sc. and Ph.D. degrees in electrical engineering from the University of Genoa, Genoa, Italy, in 1984 and 1990, respectively.

He is currently the Northern Partnership Professor of computer vision in the School of Computing, University of Dundee, Dundee, U.K. He was with the Joint Research Centre of the European Union at Ispra, University of Edinburgh and Heriot Watt University, (Edinburgh, U.K). He is the author or coauthor of about 170 refereed papers published on computer vision and its applications in manufacturing, robotics, communications and bioengineering, and coauthor of two books, one of which (with Alessandro Verri) has become a standard for computer vision (1457 citations Google Scholar at 5/5/2010). His research interests include articulated human motion tracking and medical image analysis.

Prof. Trucco has served as an Editor-in-Chief of the *Institute of Electrical Engineering Proceedings on Signal, Speech and Image Processing*, and an Editor for the *Pattern Analysis and Applications* and the IEEE TRANSACTIONS ON SYSTEMS, MAN AND CYBERNETICS C.

Hind Azegrouz (M'05) received the Master's degree in electronic engineering from École Nationale Supérieure d'Électronique, Informatique et Radiocommunications de Bordeaux, France, in 2003, and the Ph.D. degree in electrical engineering from Heriot Watt University, U.K., in 2008.

From 2008 to 2009, she was with the Image Processing Unit, Optos plc. She is currently with the Spanish National Centre of Cardiovascular Research, Madrid, Spain, where she is engaged in research on high-content screening applications. Her research interests include 2-D and 3-D biomedical image processing, optimization of high-content screening data analysis and management.

Dr. Azegrouz received a Royal Academy of Engineering Personal Grant in 2006.

Baljean Dhillon received the BMBS degree from Nottingham University, Nottingham, U.K.

He is currently a Consultant Ophthalmic Surgeon at the Princess Alexandra Eye Pavilion, Edinburgh; a part-time Professor of visual impairment research studies at Heriot Watt University, and Honorary Professor of ophthalmology at the University of Edinburgh. He is the author or coauthor of more than 150 papers published in peer-reviewed articles. He has served as an External Examiner for MD/Ph.D., IOVS MSc, Royal College of Surgeons of Edinburgh, Royal College of Surgeons of Physicians and Surgeons of Glasgow, and Royal College of Ophthalmologists. His research interests include diseases affecting the retina and macula, cataract, and age-related macula degeneration.

Dr. Dhillon is a Fellow of the Royal College of Ophthalmologists and the Royal College of Physicians and Surgeons of Glasgow.